Temporal coupled-mode theory for light scattering by an arbitrarily shaped object supporting a single resonance

Zhichao Ruan* and Shanhui Fan†

Ginzton Laboratory, Department of Electrical Engineering, Stanford University, Stanford, California 94305, USA

(Received 30 December 2011; published 18 April 2012)

We develop a temporal coupled-mode theory to describe the interaction of plane wave with an individual scatterer having an arbitrary shape. The theory involves the expansion of the fields on cylindrical or spherical wave basis for the two-dimensional and three-dimensional cases, respectively, and describes the scattering process in terms of a background scattering matrix and the resonant radiation coefficients into different cylindrical or spherical wave channels. This theory provides a general formula for the scattering and absorption cross sections. We show that for a subwavelength asymmetric scatterer with a single resonance, the scattering and absorption cross sections can exceed the single-resonance limit for some specific incident angles of illumination, but the sum of these cross sections over all angles has an upper limit. We validate the theory with numerical simulations of a metallic scatterer that does not have any rotation symmetry.

DOI: 10.1103/PhysRevA.85.043828 PACS number(s): 42.25.Fx, 03.65.Nk

I. INTRODUCTION

The study of light scattering and absorption by individual subwavelength objects, such as nanoparticle or antenna, is of great importance in nanophotonics and electromagnetics. The presence of a resonance in such an object can profoundly influence its scattering and absorption properties, resulting in having its electromagnetic cross section far exceed its geometric cross section [1], as well as complex resonance-based interference phenomena including Fano interference [2–9], all-optical analog to electromagnetically induced transparency [10–15], superscattering [16,17], and the anomalous absorption and scattering [18,19]. It is therefore of importance to develop a theoretical framework that elucidates the role of resonance in these subwavelength objects.

The temporal coupled-mode theory formalism provides a very useful general framework to study the interaction of a resonance with external waves. This formalism was initially developed and applied for analyzing waveguide-resonator interactions in integrated optics [20–22]. In these studies, the incident waves were typically expanded on the basis of propagating modes of the waveguides. This formalism has also been used to study the interaction of plane wave with grating structures [23–25], where the incident waves were expanded on a plane-wave basis. More recently, the temporal coupled-mode theory formalism with a plane-wave basis has been used to study the behavior of an individual or two slit apertures [26,27].

For the study of individual isolated objects, the cylindrical wave basis in two dimensions, or the spherical wave basis in three dimensions, provides a more natural basis for expanding the external waves. Temporal coupled-mode theory with either a cylindrical or a spherical wave expansion of the external wave has been developed in Refs. [7,28]. All these works [7,28], however, only deal with particles that have cylindrical or spherical shapes. Considering the great importance of a large number of antennas or nanoparticle structures that do not have a symmetric shape, in this paper we generalize the temporal coupled-mode theory on a cylindrical or spherical wave basis, to structures without rotational symmetry, and consider the influence of the incident angle of illumination.

The paper is organized as follows: In Sec. II we present the temporal coupled-mode theory for the two-dimensional case. We derive a general formula for the scattering matrix when the scatterer supports a single resonance. The theory is then applied to calculate the scattering and absorption cross sections, in particular for small particles with sizes far smaller than the wavelength of light. In Sec. III we compare the theoretical predictions to numerical simulations for a metallic scatterer without any rotation symmetry. Finally, we extend the theory to the three dimensions in Sec. IV.

II. THEORY

A. General scattering theory for arbitrarily shaped scatterers

We start from the general scattering theory in the two-dimensional (2D) case where a scatterer is uniform in the z direction. Consider the scatterer located at the origin, surrounding by air. When a TM wave (with its magnetic field H polarized along the z direction) impinges on the scatterer, the total field in the air region outside the scatterer can be written as

$$H_{\text{total}} = \sum_{m=-\infty}^{\infty} A_0\left[a_m^+ H_{|m|}^{(2)}(k\rho)\exp(im\theta) + a_m^- H_{|m|}^{(1)}(k\rho) \times \exp(im\theta)\right], \quad (1)$$

where (ρ,θ) is the polar coordinates oriented at the origin, k is the wave number in air, and $H_m^{(1)}$ ($H_m^{(2)}$) is the mth order Hankel function of the first (second) kind. Here we take the convention that the field varies in time as $\exp(-i\omega t)$. So a_m^+ and a_m^- can be identified as the incoming and outgoing wave amplitudes, respectively. With the choice of

$$A_0 = \sqrt{\frac{\omega\varepsilon_0}{2}}, \quad (2)$$

*zhichao@stanford.edu
†shanhui@stanford.edu

$|a_m^+|^2$ and $|a_m^-|^2$ represent the power of the incoming and outgoing cylindrical waves in the mth channel and have the unit of W/m [7]. Therefore, the total powers carried by incoming and outgoing waves are

$$P^{\pm} = \sum_{m=-\infty}^{\infty} |a_m^{\pm}|^2 = (\mathbf{a}^{\pm})^{\dagger}\mathbf{a}^{\pm}, \tag{3}$$

where $\mathbf{a}^{\pm}$ is a column vector composed by $a_m^{\pm}$ as

$$\mathbf{a}^{\pm} = \begin{bmatrix} \vdots \\ a_{-1}^{\pm} \\ a_0^{\pm} \\ a_1^{\pm} \\ \vdots \end{bmatrix}. \tag{4}$$

Following Refs. [29,30] we define a scattering matrix $\mathbf{S}$ that connects $\mathbf{a}^-$ with $\mathbf{a}^+$ as

$$\mathbf{a}^- = \mathbf{S}\mathbf{a}^+. \tag{5}$$

When the scatterer is lossless, by energy conservation, $\mathbf{S}$ is unitary, that is,

$$\mathbf{S}^{\dagger}\mathbf{S} = \mathbf{I}. \tag{6}$$

In addition, if the system satisfies time-reversal symmetry, $\mathbf{S}$ needs to be further constrained. A time-reversal operation transforms an outgoing (incoming) wave in the channel m to an incoming (outgoing) wave in the channel $(-m)$. Thus, for an outgoing wave described by $\mathbf{a}^-$, its time-reversed counterpart is an incoming wave:

$$\tilde{\mathbf{a}}^+ = \hat{O}\mathbf{a}^{-*}. \tag{7}$$

Similarly, the time-reversed counterpart of an incoming wave described by $\mathbf{a}^+$ is

$$\tilde{\mathbf{a}}^- = \hat{O}\mathbf{a}^{+*}. \tag{8}$$

Here $\hat{O}_{mn} = \delta_{m,-n}$ and $\hat{O}$ has a matrix form:

$$\hat{O} = \begin{bmatrix} 0 & & & & \iddots \\ & & & 1 & \\ & & 1 & & \\ & 1 & & & \\ \iddots & & & & 0 \end{bmatrix}. \tag{9}$$

For the given set of incoming and outgoing waves satisfying Eq. (5), if the system has time-reversal symmetry, we should also have from Eqs. (7) and (8)

$$\tilde{\mathbf{a}}^- = \mathbf{S}\tilde{\mathbf{a}}^+ \tag{10}$$

and therefore

$$\mathbf{S}^{-1} = \hat{O}\mathbf{S}^*\hat{O}. \tag{11}$$

Combining Eqs. (6) and (11), we see that in a system that conserves energy and has time-reversal symmetry, $\mathbf{S}$ should satisfy

$$\mathbf{S}^T = \hat{O}\mathbf{S}\hat{O}. \tag{12}$$

B. Temporal coupled-mode theory in the single-resonance case

We now apply the temporal coupled-mode theory to calculate $\mathbf{S}$ for the case when the scatterer supports a single resonant mode. We consider the amplitude c of the resonance normalized such that $|c|^2$ corresponds to the energy inside the resonator [20] with the unit of J/m, which is appropriate for 2D systems. Using the temporal coupled-mode theory formalism [20,24], the dynamic equation for the amplitude c is

$$\frac{dc}{dt} = (-i\omega_0 - \gamma_0 - \gamma)\,c + \boldsymbol{\kappa}^T\mathbf{a}^+, \tag{13a}$$

$$\mathbf{a}^- = \mathbf{B}\mathbf{a}^+ + c\mathbf{d}, \tag{13b}$$

where ω_0 is the resonant frequency, γ_0 is the intrinsic loss rate due to, for example, material absorption, γ is the external leakage rate due to the coupling of the resonance to the outgoing wave, and $\boldsymbol{\kappa}$ corresponds to the coupling coefficients between the resonance and the incoming wave. Note that such coupled-mode formalism is, strictly speaking, valid only when $\gamma_0 + \gamma \ll \omega_0$ [20].

As shown in Eq. (13b) the outgoing waves have contributions from two pathways. The direct pathway, as described by the term $\mathbf{B}\mathbf{a}^+$, forms the background in the response spectrum. $\mathbf{B}$ is the background scattering matrix. In this pathway, scattering occurs without exciting the resonance. The indirect, or the resonant, pathway is described by the term $c\mathbf{d}$. The vector $\mathbf{d}$ can be determined by considering the scenario, where the resonance has amplitude c, and there is no incoming wave, that is, $\mathbf{a}^+ = \mathbf{0}$. For this scenario, the radiation field outside the scatterer can be written as

$$H_{\text{eigen}} = c\sum_{m=-\infty}^{\infty} A_0 d_m H_{|m|}^{(1)}(k\rho)\exp(il\theta). \tag{14}$$

Here d_m, which are components of the column vector $\mathbf{d}$, correspond to the radiation coefficients of the resonance.

From Eqs. (13) we have the scattering matrix for the single-resonance scatterer as

$$\mathbf{S} = \mathbf{B} + \frac{\mathbf{d}\boldsymbol{\kappa}^T}{i\omega_0 - i\omega + \gamma + \gamma_0}. \tag{15}$$

C. Relations among B, d, and κ

We now derive constrains between $\mathbf{B}$, $\mathbf{d}$, and $\boldsymbol{\kappa}$ as imposed by energy conservation and time-reversal symmetry [24]. Let us first consider the lossless case with $\gamma_0 = 0$. $\mathbf{B}$ and $\mathbf{S}$ should then both satisfy Eq. (12). As a result we have

$$\boldsymbol{\kappa}\mathbf{d}^T = \hat{O}\mathbf{d}\boldsymbol{\kappa}^T\hat{O}. \tag{16}$$

Next, we consider a scenario that the incoming wave is absent (i.e., $\mathbf{a}^+ = \mathbf{0}$). From Eqs. (13) we have

$$c = c(0)\exp(-i\omega_0 t - \gamma t), \tag{17a}$$

$$\mathbf{a}^- = c(0)\exp(-i\omega_0 t - \gamma t)\,\mathbf{d}, \tag{17b}$$

where $c(0)$ is the resonance amplitude at $t = 0$. According to energy conservation, the energy leakage rate must be equal to

the power of the outgoing wave, that is,

$$\frac{\mathrm{d}|c|^2}{\mathrm{d}t} = -2\gamma|c|^2 = -(\mathbf{a}^-)^\dagger\mathbf{a}^- = -\mathbf{d}^\dagger\mathbf{d}|c|^2, \tag{18}$$

which requires that

$$\mathbf{d}^\dagger\mathbf{d} = 2\gamma. \tag{19}$$

Now let us perform a time-reversal transformation. In this scenario, the original outgoing wave in the mth channel with the exponential decay will be transformed to the incoming wave in the $(-m)$th channel with an exponentially growing amplitude. Such an exponentially growing excitation results in a resonant amplitude that also grows exponentially, without the outgoing wave. So in the time-reversed case, the amplitude of the resonance $\tilde{c}$ and the incoming wave amplitude $\tilde{\mathbf{a}}^+$ can be written as

$$\tilde{c} = [c(-t)]^*, \tag{20a}$$
$$\tilde{\mathbf{a}}^+ = \hat{O}[\mathbf{a}^-(-t)]^*, \tag{20b}$$

where c and $\mathbf{a}^-$ are described by the original case represented in Eqs. (17). Substituting Eqs. (20) into Eqs. (13) we have

$$\boldsymbol{\kappa}^T\hat{O}\mathbf{d}^* = 2\gamma, \tag{21}$$
$$\mathbf{B}\hat{O}\mathbf{d}^* + \mathbf{d} = 0. \tag{22}$$

By left multiplying $\mathbf{d}^*$ on both sides of Eq. (16) and applying Eqs. (19) and (21), we find

$$\boldsymbol{\kappa} = \hat{O}\mathbf{d}. \tag{23}$$

From Eqs. (15) and (23) we have a general form of the scattering matrix

$$\mathbf{S} = \mathbf{B} + \frac{\mathbf{d}\mathbf{d}^T\hat{O}}{i\omega_0 - i\omega + \gamma + \gamma_0}. \tag{24}$$

Below we will apply Eq. (24) to describe the scattering process of a single particle.

D. Scattering and absorption cross sections

Generally, for a scatterer without rotation symmetry the scattering and absorption cross sections are functions of incident angle. We consider a plane wave with $H_{\mathrm{inc}} = H_0\exp(i\mathbf{k}\cdot\mathbf{r})$ incident upon the scatterer with an incident angle of ϕ schematically showed in Fig. 1. Here $\mathbf{k}$ is the wave vector of the incident plane wave. The total field in the air region outside the scatterer is then written as

$$H_{\mathrm{total}} = H_0\exp(i\mathbf{k}\cdot\mathbf{r}) + \sum_{m=-\infty}^{\infty} A_0 s_m H^{(1)}_{|m|}(k\rho)\exp(im\theta), \tag{25}$$

where s_m is the amplitude of the scattered field in the mth channel. To connect Eq. (25) with Eq. (1), we expand the plane wave into cylindrical waves as

$$\exp(i\mathbf{k}\cdot\mathbf{r}) = \sum_{m=-\infty}^{\infty} i^{|m|}\exp(-i\phi m)\left(\frac{H^{(2)}_{|m|}(k\rho) + H^{(1)}_{|m|}(k\rho)}{2}\right) \times \exp(im\theta).$$

In comparison with Eq. (1), we then have

$$a_m^+ = \sqrt{\frac{2}{\omega\varepsilon_0}}H_0 f_m, \tag{26}$$
$$a_m^- = a_m^+ + s_m, \tag{27}$$

where

$$f_m = \frac{i^{|m|}}{2}\exp(-i\phi m). \tag{28}$$

Below we will use the symbols $\mathbf{f}$, $\mathbf{a}^+$, $\mathbf{a}^-$, and $\mathbf{s}$ to denote the column vectors with components f_m, a_m^+, a_m^-, and s_m defined above, respectively.

We define a matrix[1] $\mathbf{L}$ that connects $\mathbf{s}$ and $\mathbf{a}^+$ as $\mathbf{s} = \mathbf{L}\mathbf{a}^+$, and applying Eq. (27) we have

$$\mathbf{L} = \mathbf{S} - \mathbf{I}. \tag{29}$$

As a result, the total scattered and absorbed powers are

$$P_{\mathrm{sct}} = \mathbf{s}^\dagger\mathbf{s} = (\mathbf{a}^+)^\dagger\mathbf{L}^\dagger\mathbf{L}\mathbf{a}^+, \tag{30a}$$
$$P_{\mathrm{abs}} = (\mathbf{a}^+)^\dagger\mathbf{a}^+ - (\mathbf{a}^-)^\dagger\mathbf{a}^- = (\mathbf{a}^+)^\dagger(\mathbf{I} - \mathbf{S}^\dagger\mathbf{S})\mathbf{a}^+. \tag{30b}$$

Following the definition of the scattering and absorption cross section as $C_{\mathrm{sct}} \equiv P_{\mathrm{sct}}/I_0$ and $C_{\mathrm{abs}} \equiv P_{\mathrm{abs}}/I_0$, where $I_0 = \frac{1}{2}\sqrt{\frac{\mu_0}{\varepsilon_0}}|H_0|^2$ is the intensity of the incident plane wave, we have

$$C_{\mathrm{sct}} = \frac{2\lambda}{\pi}\mathbf{f}^\dagger\mathbf{L}^\dagger\mathbf{L}\mathbf{f}, \tag{31a}$$
$$C_{\mathrm{abs}} = \frac{2\lambda}{\pi}\mathbf{f}^\dagger(\mathbf{I} - \mathbf{S}^\dagger\mathbf{S})\mathbf{f}. \tag{31b}$$

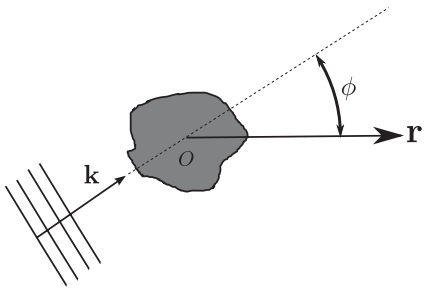

FIG. 1. A plane wave impinges upon a scatterer with an incident angle of ϕ. The scatterer does not have rotational symmetry.

E. Approximation of background scattering matrix for small scatterer

When the scatterer is much smaller than the wavelength, there is no scattering contribution from the direct pathway. In this case, the background scattering matrix $\mathbf{B}$ can be approximated as

$$\mathbf{B} = \mathbf{I},$$

[1]Note that the matrix $\mathbf{L}$ is different from the T matrix defined in Refs. [29,30].

and therefore

$$\mathbf{L} = \frac{\mathbf{d}\mathbf{d}^T \hat{O}}{i\omega_0 - i\omega + \gamma + \gamma_0}. \tag{32}$$

Thus, the amplitudes for the scattered field are

$$\mathbf{s} = \mathbf{L}\mathbf{a}^+ = \frac{\mathbf{d}^T \hat{O}\mathbf{a}^+}{i\omega_0 - i\omega + \gamma + \gamma_0}\mathbf{d}. \tag{33}$$

Equation (33) shows that the scattered field has the same angular distribution as the radiation coefficients of the resonance mode. The angular distribution of the scattered field is therefore independent of the incident angle.

Furthermore, from Eq. (22) the resonant radiation coefficients are constrained by

$$\hat{O}\mathbf{d}^* = -\mathbf{d}, \tag{34}$$

that is, ${d_{-m}}^* = -d_m$. By applying Eqs. (32) and (34) into Eqs. (31), the scattering and absorption cross sections can be simplified as

$$C_{\text{sct}} = \frac{2\lambda}{\pi}\frac{2\gamma}{(\omega_0 - \omega)^2 + (\gamma + \gamma_0)^2}|\mathbf{d}^\dagger \mathbf{f}|^2, \tag{35a}$$

$$C_{\text{abs}} = \frac{2\lambda}{\pi}\frac{2\gamma_0}{(\omega_0 - \omega)^2 + (\gamma + \gamma_0)^2}|\mathbf{d}^\dagger \mathbf{f}|^2. \tag{35b}$$

Equations (35a) and (35b) show that for a small scatterer supporting a single resonance, the cross section spectra always have a Lorentzian line shape, and the maximum cross sections occur at the resonant frequency. The resonance linewidth is determined by the leakage rate and the intrinsic loss rate.

F. Angular sum rule for the scattering and absorption cross sections of small scatterers

For a scatterer without cylindrical symmetry, as we vary the angle of incidence ϕ as shown in Fig. 1, the scattering and absorption cross sections will vary as a function of ϕ. However, below we show that the such a variation is constraint by an angular sum rule.

To prove the angular sum rule, we note that starting from Eq. (28) we have

$$\int_0^{2\pi} (\mathbf{d}^T \mathbf{f})^\dagger (\mathbf{d}^T \mathbf{f}) d\phi = \frac{\pi}{2}\|\mathbf{d}\|^2 = \pi\gamma,$$

where the column vectors $\mathbf{f}$ depend on the angle of incidence ϕ as shown in Eq. (28). Consequently, integrating Eqs. (35) over ϕ, we have the angular sum rule for the scattering and absorption cross sections:

$$\int_0^{2\pi} C_{\text{sct}} d\phi = 4\lambda \frac{\gamma^2}{(\omega_0 - \omega)^2 + (\gamma + \gamma_0)^2}, \tag{36a}$$

$$\int_0^{2\pi} C_{\text{abs}} d\phi = 4\lambda \frac{\gamma_0\gamma}{(\omega_0 - \omega)^2 + (\gamma + \gamma_0)^2}. \tag{36b}$$

Equations (36) show that the sum of the scattering and absorption cross sections over all angles has maxima of 4λ and λ at the resonant frequency, when $\gamma_0 = 0$ and $\gamma_0 = \gamma$, respectively. A similar result has been derived for the transmission cross section of a single metallic slit aperture [26].

Moreover, Eqs. (36) indicate the difference of the scattering property between a rotationally symmetric scatterer and an asymmetric scatterer. For a rotationally symmetric scatterer with a single resonance, the scattering and absorption cross sections are both independent of the incident angle, and have maxima of $2\lambda/\pi$ and $\lambda/2\pi$, respectively. In contrast, the electromagnetic cross section of a small nonsymmetric scatterer can exceed such a limit for some specific incident angles. We note that the existence of such a sum rule is a direct consequence of having only a single resonance. One could overcome the constraint here by aligning multiple resonances at the same frequency, as shown in Refs. [16,17].

III. NUMERICAL VALIDATION

To validate of our theory we compare the theoretical predictions to numerical simulations of a metallic scatterer that has no rotation symmetry. Figure 2 shows the schematic of the scatterer, where the dark and light gray parts correspond to the metal and dielectric regions, respectively. The permittivity of dielectric is $\varepsilon_d = 12.96$, and the metal is described by a Drude model $\varepsilon_m = 1 - \omega_p^2/(\omega^2 + i\gamma_d\omega)$, where ω_p and γ_d are the plasma frequency and the damping rate, respectively.

We first make the comparison for the lossless case where $\gamma_d = 0$. For this purpose we first use a mode-solving routine in a finite element method (FEM) package[2] to calculate the the frequency and leakage rate of a resonance in the scatterer. The structure in Fig. 2(a) has a resonant mode at the frequency of $\omega_0 = 0.14417\omega_p$, and the external leakage rate of the resonant mode is $\gamma = 1.2065 \times 10^{-4}\omega_p$. Figure 2(b) shows the H_z field distribution of the resonant mode.

To apply the temporal coupled-mode theory, we need to identify the resonant radiation coefficients $\mathbf{d}$ and the background scattering matrix $\mathbf{B}$ for this system. Since the size of the scatterer is less than one tenth of the wavelength, we adopt the small-scatterer approximation that $\mathbf{B} = \mathbf{I}$. This approximation will be explicitly validated below.

To determine the resonant radiation coefficients $\mathbf{d}$, we first expand the resonant radiation field into cylindrical waves in a form as shown in Eq. (14). We note that numerically determined radiation field has an arbitrary overall complex amplitude as seen in Eq. (14). However, the norm of $\mathbf{d}$ is related to the leakage rate of the resonance Eq. (19). Also, we recall from Eq. (34) that $d_m = -{d_{-m}}^*$, thus d_0 is purely imaginary. These two constraints are sufficient to allow us to fix the overall complex amplitude of the radiation field, and hence d_m for all m.

For this structure in Figs. 2(a) and 2(c) shows the amplitude and the phase of the resonant radiation coefficients d_m thus determined for the order $-5 \leqslant m \leqslant 5$, respectively. The amplitudes of d_m are significant for $-2 \leqslant m \leqslant 2$. Therefore the resonance cannot be approximated as either a monopole or a dipole mode. Also, since the resonant mode has even symmetry about the x axis, d_m should satisfy $d_m = d_{-m}$. Therefore all d_m with $m \neq 0$ should be purely imaginary. In Fig. 2(c) we indeed observe that the phases of all the d_m with $m \neq 0$ that have significant amplitudes are close to $\pi/2$, consistent with

[2]Here we use the commercial software COMSOL.

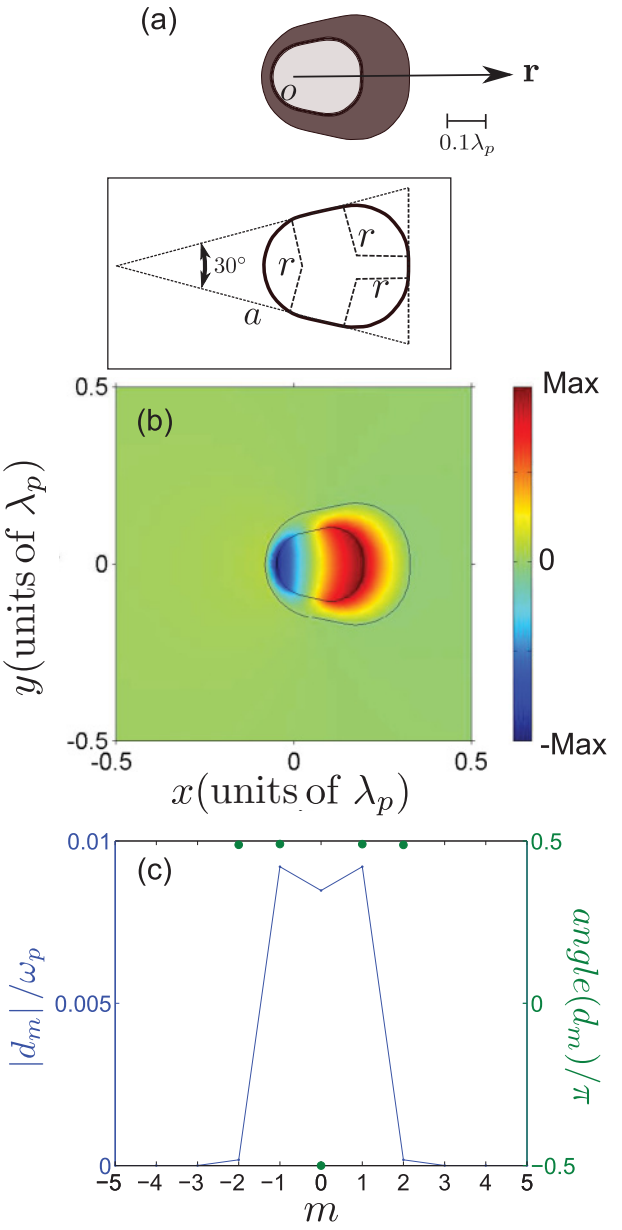

FIG. 2. (Color online) (a) Schematic of a scatterer with a rounded-corner triangle shape. The dark and light gray areas correspond to a plasmonic metal and a dielectric, respectively. The permittivity of dielectric is $\varepsilon_d = 12.96$, and the metal is described by a Drude model $\varepsilon_m = 1 - \omega_p^2/(\omega^2 + i\gamma_d\omega)$. Here λ_p corresponds to the plasmon wavelength of $2\pi c/\omega_p$, where c is the velocity of light in vacuum. Inset: We generate the outer boundary of the scatterer by rounding corners of an isosceles triangle with a tip angle of 30°. The equal sides of the triangle and the radius of the round corner are $a = 1\lambda_p$ and $r = 0.15\lambda_p$, respectively. The inner boundary is created by scaling the outer boundary by a factor of 0.6. (b) The real part of H_z field for the resonant mode at the frequency of $\omega_0 = 0.14417\omega_p$. (c) The amplitude (solid line) and phase (dotted line) of the resonant radiation coefficient d_m.

the requirements for both the mirror symmetry and the small-particle approximation in the temporal coupled-mode theory.

Having determined all the parameters in the temporal coupled-mode theory, we now compare the prediction of

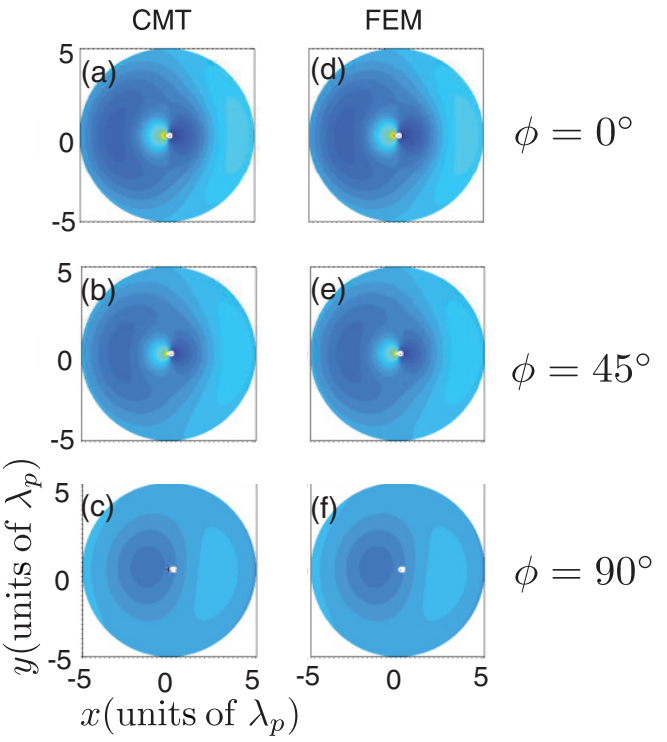

FIG. 3. (Color online) (a)–(c) The amplitude of the scattering field calculated by the temporal coupled-mode theory (CMT) for a plane wave with the incident angles of $\phi = 0°$, 45°, and 90°. (d)–(f) The results from the FEM solver.

this theory to the numerical calculations of scattering and absorption cross sections of this system. We first compare the scattered fields for three different incident angles $\phi = 0°$, 45°, and 90°, with the incident wave at the resonant frequency. We see excellent agreement between the results from temporal coupled-mode theory [Figs. 3(a)–3(c)], and the numerical calculations [Figs. 3(d)–3(f)].

For a small scatterer, with the assumption of $\mathbf{B} = \mathbf{I}$, the scattered field is solely determined by the radiation field of the resonant mode, which is independent of the angle of incidence, as shown in Eq. (33). Numerically we indeed see

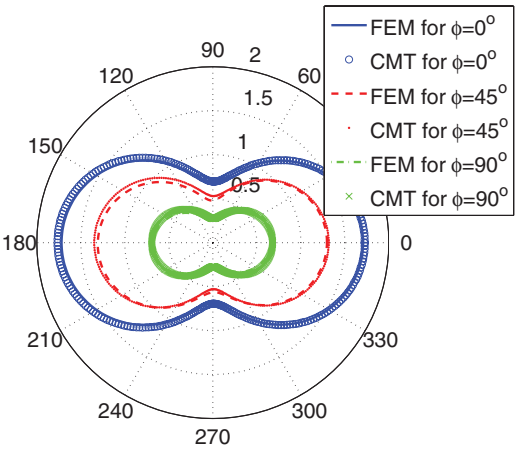

FIG. 4. (Color online) The far-field amplitude of the scattering field for a plane wave with the incident angles of $\phi = 0°$, 45°, and 90°.

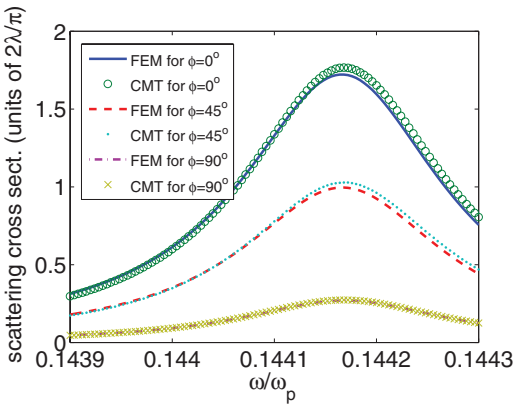

FIG. 5. (Color online) The scattering cross section spectra of the lossless scatterer for three different incident angles $\phi = 0^\circ$, 45°, and 90°.

that the scattered field has the same angular distribution from the different angle of incidence we consider here, in agreement with the temporal coupled-mode theory analysis (Fig. 4).

In Fig. 5 we compare the spectra of the scattering cross sections for the three angles of incidence, and again obtain excellent agreement between the theory and the FEM simulations. Moreover, we observe that the scattering cross section for this structure decreases the angle of incidence increase. This is consistent with the results in Fig. 4, which shows that the coupling between the incoming wave and the resonance decreases with the increasing incident angle.

Finally we check the theory for the lossy case. Here we set that the damping rate of the plasmonic material is $\gamma_p = 0.0001\omega_p$. The solid and dashed lines in Fig. 6 correspond to the spectra of the scattering and absorption cross sections for the normal incident case through the FEM calculation. By fitting these curves through Eq. (35a), we obtain that a resonant frequency for the the lossy case is still $\omega_0 = 0.144167\omega_p$, and $\gamma_0 + \gamma$ is $1.6857 \times 10^{-4}\omega_p$. Here we assume that the resonant radiation coefficients and the external leakage rate of the resonant mode do not change from the lossless case. So the intrinsic loss rate is $\gamma_0 = 4.802 \times 10^{-5}\omega_p$. The cross section spectra by the coupled-mode theory are plotted as the circle and dotted lines in Fig. 6. It shows that there is also

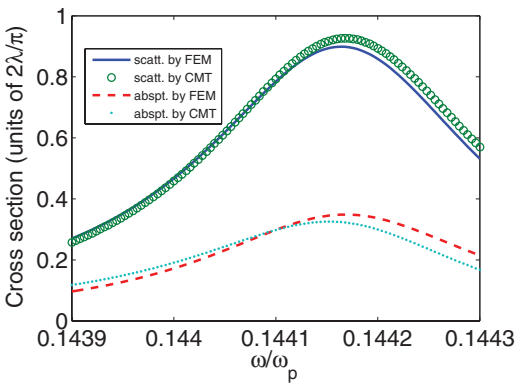

FIG. 6. (Color online) The spectra of the scattering and absorption cross sections for the lossy scatterer with the damping rate $\gamma_d = 0.0001\omega_p$.

a good agreement between the coupled-mode theory and the FEM results in the lossy case.

To summarize this section, we obtain excellent agreements between the temporal coupled-mode theory formulas and exact electromagnetic simulations. We emphasize that the agreements here are not a curve fit of theoretical results to numerical simulations. Instead, to determine the parameters for the temporal coupled-mode theory, only a single calculation on the resonance mode is needed. (For the lossy case, two calculations on the resonant modes are required in order to separate out γ and γ_0.) The temporal coupled-mode theory can then be used to reliably predict the behavior of the structure over all angles of incidence, and for all frequencies in the vicinity of the resonant frequency, with no further need for numerical simulations. Thus, the use of temporal coupled-mode theory can greatly simplify the task for computational characterization of the scattering and absorption properties of a small particle, and provide important insights regarding the behaviors of these particles in general.

IV. THE THEORY FOR SCATTERING IN THREE DIMENSIONS

We now adapt the above theory to three-dimensional (3D) cases. Instead of cylindrical waves used in the 2D case, the total field in the 3D case is expanded on the basis of spherical waves labeled by (l,m,σ). Here l is the total angular momentum, m corresponds to the angular momentum component along the z direction and is subject to $-l \leqslant m \leqslant l$, and σ labels polarizations. At each angular momentum (l,m), there are two orthogonal polarizations: transverse magnetic (TM) and transverse electric (TE). The total electric and magnetic field outside the scatterer are the superposition of these two polarizations and can be written as

$$\mathbf{E} = \mathbf{E}_{\mathrm{TE}} - \frac{1}{i\omega\varepsilon_0}\nabla \times \mathbf{H}_{\mathrm{TM}}, \tag{37}$$

$$\mathbf{H} = \frac{1}{i\omega\mu_0}\nabla \times \mathbf{E}_{\mathrm{TE}} + \mathbf{H}_{\mathrm{TM}}, \tag{38}$$

where $\mathbf{E}_{\mathrm{TE}}$ ($\mathbf{H}_{\mathrm{TM}}$) is the transverse electric (magnetic) field. $\mathbf{H}_{\mathrm{TM}} = \sqrt[4]{\frac{\varepsilon_0}{\mu_0}}\nabla \times \hat{\mathbf{r}}\Phi_{\mathrm{TM}}$ and $\mathbf{E}_{\mathrm{TE}} = \sqrt[4]{\frac{\mu_0}{\varepsilon_0}}\nabla \times \hat{\mathbf{r}}\Phi_{\mathrm{TE}}$. Here Φ_{TM} (Φ_{TE}) is the electric (magnetic) potential and satisfies the scalar wave equation in the spherical coordinate [31]:

$$\Phi_\sigma = \sum_{l=1}^{\infty}\sum_{m=-l}^{l} A_{l,m}\left[a^+_{l,m,\sigma}h^{(2)}_l(kr) + a^-_{l,m,\sigma}h^{(1)}_l(kr)\right] \times P^{|m|}_l(\cos\theta)\exp(im\phi), \tag{39}$$

where $a^+_{l,m,\sigma}$ and $a^-_{l,m,\sigma}$ are, respectively, the incoming and outgoing wave amplitudes, (r,θ,ϕ) are the spherical coordinates oriented at the center, k is the wave number in air, $h^{(1)}_l$ ($h^{(2)}_l$) is the lth order spherical Hankel function of the first (second) kind, and P^m_l is the associated Legendre function of the first kind. With the choice of the normalization constant as

$$A_{l,m} = k\sqrt{\frac{1}{2\pi}\frac{(2l+1)}{l(l+1)}\frac{(l-|m|)!}{(l+|m|)!}}, \tag{40}$$

$|a^+_{l,m,\sigma}|^2$ and $|a^-_{l,m,\sigma}|^2$ represent the power of the incoming and outgoing spherical waves in the (l,m,σ)th channel with the

unit of Watt [17]. When a scatterer supports a single resonant mode, the potential for the radiation field can be written as

$$\Phi_\sigma^{\text{eigen}} = c\sum_{l=1}^{\infty}\sum_{m=-l}^{l} A_{l,m} d_{l,m,\sigma} h_l^{(1)}(kr) P_l^{|m|}(\cos\theta)\exp(im\phi), \tag{41}$$

where c corresponds to the amplitude of the resonance. Similar to the 2D case, here we will define a vector $\mathbf{d}$ with its components being the resonant radiation coefficients $d_{l,m,\sigma}$.

Now we consider a plane wave with an electric field $\mathbf{E}_{\text{inc}} = E_0\hat{\mathbf{e}}_{\text{inc}}\exp(i\mathbf{k}\cdot\mathbf{r})$ incident upon a scatterer. By an expansion onto the basis of spherical waves, the incident field can be described by a potential as

$$\Phi_\sigma^{\text{inc}} = \sum_{l=1}^{\infty}\sum_{m=-l}^{l} A_{l,m} g_{l,m,\sigma} j_l(kr) P_l^{|m|}(\cos\theta)\exp(im\phi), \tag{42}$$

where j_l is the lth order spherical Bessel function. The expansion coefficients $g_{l,m,\sigma}$ are

$$g_{l,m,\sigma} = \lambda\sqrt[4]{\frac{\varepsilon_0}{\mu_0}}\sqrt{\frac{1}{2\pi}} E_0 f_{l,m,\sigma}, \tag{43}$$

where $f_{l,m,\sigma}$ are

$$f_{l,m,\text{TM}} = -\sqrt{\frac{(2l+1)}{l(l+1)}\frac{(l-|m|)!}{(l+|m|)!}} i^l \hat{\mathbf{e}}_{\text{inc}}\cdot\mathbf{B}_{-ml}(\theta_i,\phi_i), \tag{44a}$$

$$f_{l,m,\text{TE}} = \sqrt{\frac{(2l+1)}{l(l+1)}\frac{(l-|m|)!}{(l+|m|)!}} i^l \hat{\mathbf{e}}_{\text{inc}}\cdot\mathbf{C}_{-ml}(\theta_i,\phi_i). \tag{44b}$$

θ_i and ϕ_i are the azimuth and horizon angle of the incident wave vector, respectively, and the vectors $\mathbf{B}$ and $\mathbf{C}$ are [29]

$$\mathbf{B}_{ml} = \left[\frac{d}{d\theta}P_l^{|m|}(\cos\theta)\hat{\mathbf{e}}_\theta + \frac{im}{\sin\theta}P_l^{|m|}(\cos\theta)\hat{\mathbf{e}}_\phi\right]\exp(im\phi), \tag{45a}$$

$$\mathbf{C}_{ml} = \left[\frac{im}{\sin\theta}P_l^{|m|}(\cos\theta)\hat{\mathbf{e}}_\theta - \frac{d}{d\theta}P_l^{|m|}(\cos\theta)\hat{\mathbf{e}}_\phi\right]\exp(im\phi). \tag{45b}$$

Correspondingly, the scattered field $\mathbf{E}_{\text{sct}}$ can be described by a potential as

$$\Phi_\sigma^{\text{sct}} = \sum_{l=1}^{\infty}\sum_{m=-l}^{l} A_{l,m} s_{l,m,\sigma} h_l^{(1)}(kr) P_l^{|m|}(\cos\theta)\exp(im\phi), \tag{46}$$

where $s_{l,m,\sigma}$ corresponds to the amplitude of the scattered field. Therefore, for the total field $\mathbf{E}_{\text{tot}} = \mathbf{E}_{\text{inc}} + \mathbf{E}_{\text{sct}}$, the coefficients of the incoming and outing waves are

$$a^+_{l,m,\sigma} = \frac{g_{l,m,\sigma}}{2}, \tag{47a}$$

$$a^-_{l,m,\sigma} = \frac{g_{l,m,\sigma}}{2} + s_{l,m,\sigma}. \tag{47b}$$

Having defined the incoming and outgoing wave amplitudes in the spherical basis, the temporal coupled-mode equations (13), the theoretical constraints on the parameters of the temporal coupled-mode theory Eqs. (19) and (23), and the general form of the scattering matrix Eq. (24), can now all be directly applied to the three-dimensional case. Using the definition of the scattering and absorption cross sections: $C_{\text{sct}} \equiv P_{\text{sct}}/I_0$ and $C_{\text{abs}} \equiv P_{\text{abs}}/I_0$, where $I_0 = \frac{1}{2}\sqrt{\varepsilon_0/\mu_0}|E_0|^2$ is the intensity of the incident plane wave, we have

$$C_{\text{sct}} = \frac{\lambda^2}{4\pi}\mathbf{f}^\dagger\mathbf{L}^\dagger\mathbf{L}\mathbf{f}, \tag{48a}$$

$$C_{\text{abs}} = \frac{\lambda^2}{4\pi}\mathbf{f}^\dagger(\mathbf{I} - \mathbf{S}^\dagger\mathbf{S})\mathbf{f}. \tag{48b}$$

Here $\mathbf{f}$ is a column vector with components $f_{l,m,\sigma}$ defined in Eqs. (44), and the scattering matrix $\mathbf{S}$ and the matrix $\mathbf{L}$ have the same form as the two-dimensional case of Eqs. (24) and (29).

V. SUMMARY AND OUTLOOK

In summary, we show that on the basis of cylindrical (spherical) waves in the 2D (3D) case, the light scattering by arbitrarily shaped scatterer with a single resonance can be modeled by a temporal coupled-mode theory formalism. By introducing the background scattering matrix and the resonant radiation coefficients, the light scattering response for any incident angle or wave shape can be directly evaluated, which provides a general formula for the scattering and absorption cross sections. We validate the analysis with numerical simulations for a metallic scatterer that does not have any rotation symmetry.

We note that the present theory can be generalized for scatterers supporting multiple resonances. In this case, the dynamics of the multiple resonances are described by a matrix [32]. The off-diagonal term of the matrix is in part determined by the overlap between the radiation pattern of resonances, and can be directly evaluated from the resonant radiation coefficients for each resonance.

ACKNOWLEDGMENTS

The authors thank L. Verslegers, Z. Yu, and P. B. Catrysse for helpful discussions. This work is supported by the Interconnect Focus Center, funded under the Focus Center Research Program (FCRP), a Semiconductor Research Corporation entity, and DOE Grant No. DE-FG 07ER46426.

[1] M. Husnik, M. W. Klein, N. Feth, M. König, J. Niegemann, K. Busch, S. Linden, and M. Wegener, Nat. Photon. **2**, 614 (2008).

[2] N. J. Halas, S. Lal, W. S. Chang, S. Link, and P. Nordlander, Chem. Rev. **111**, 3913 (2011).

[3] B. Luk'yanchuk, N. I. Zheludev, S. A. Maier, N. J. Halas, P. Nordlander, H. Giessen, and C. T. Chong, Nat. Mater. **9**, 707 (2010).

[4] A. E. Miroshnichenko, S. Flach, and Y. S. Kivshar, Rev. Mod. Phys. **82**, 2257 (2010).

[5] R. D. Artuso and G. W. Bryant, Nano Lett. **8**, 2106 (2008).
[6] A. Christ, O. J. F. Martin, Y. Ekinci, N. A. Gippius, and S. G. Tikhodeev, Nano Lett. **8**, 2171 (2008).
[7] Z. Ruan and S. Fan, J. Phys. Chem. C **114**, 7324 (2009).
[8] F. Hao, P. Nordlander, Y. Sonnefraud, P. V. Dorpe, and S. A. Maier, ACS Nano **3**, 643 (2009).
[9] B. Gallinet and O. J. F. Martin, Phys. Rev. B **83**, 235427 (2011).
[10] N. Papasimakis, V. A. Fedotov, N. I. Zheludev, and S. L. Prosvirnin, Phys. Rev. Lett. **101**, 253903 (2008).
[11] S. Zhang, D. A. Genov, Y. Wang, M. Liu, and X. Zhang, Phys. Rev. Lett. **101**, 047401 (2008).
[12] P. Tassin, L. Zhang, T. Koschny, E. N. Economou, and C. M. Soukoulis, Phys. Rev. Lett. **102**, 053901 (2009).
[13] V. A. Fedotov, M. Rose, S. L. Prosvirnin, N. Papasimakis, and N. I. Zheludev, Phys. Rev. Lett. **99**, 147401 (2007).
[14] S. Y. Chiam, R. Singh, C. Rockstuhl, F. Lederer, W. Zhang, and A. A. Bettiol, Phys. Rev. B **80**, 153103 (2009).
[15] N. Liu, L. Langguth, T. Weiss, J. Kastel, M. Fleischhauer, T. Pfau, and H. Giessen, Nat. Mater. **8**, 758 (2009).
[16] Z. Ruan and S. Fan, Phys. Rev. Lett. **105**, 013901 (2010).
[17] Z. Ruan and S. Fan, Appl. Phys. Lett. **98**, 043101 (2011).
[18] M. I. Tribelsky and B. S. Lukȳanchuk, Phys. Rev. Lett. **97**, 263902 (2006).
[19] M. Tribelsky, Europhys. Lett. **94**, 14004 (2011).
[20] H. Haus, *Waves and Fields in Optoelectronics* (Prentice-Hall, Englewood Cliffs, NJ, 1984).
[21] C. Manolatou, M. J. Khan, S. Fan, P. R. Villeneuve, H. A. Haus, and J. D. Joannopoulos, IEEE J. Quantum Electron. **35**, 1322 (1999).
[22] A. Chutinan, M. Mochizuki, M. Imada, and S. Noda, Appl. Phys. Lett. **79**, 2690 (2001).
[23] S. Fan and J. D. Joannopoulos, Phys. Rev. B **65**, 235112 (2002).
[24] S. Fan, W. Suh, and J. D. Joannopoulos, J. Opt. Soc. Am. A **20**, 569 (2003).
[25] Z. Yu, A. Raman, and S. Fan, Proc. Natl. Acad. Sci. USA **107**, 17491 (2010).
[26] L. Verslegers, Z. Yu, P. B. Catrysse, and S. Fan, J. Opt. Soc. Am. B **27**, 1947 (2010).
[27] L. Verslegers, Z. Yu, Z. Ruan, P. B. Catrysse, and S. Fan, Phys. Rev. Lett. **108**, 083902 (2012).
[28] R. E. Hamam, A. Karalis, J. D. Joannopoulos, and M. Soljačić, Phys. Rev. A **75**, 053801 (2007).
[29] L. Tsang, J. A. Kong, K. H. Ding, and C. O. Ao, *Scattering of Electromagnetic Waves: Theories and Applications* (Wiley, New York, 2000).
[30] M. I. Mishchenko, L. D. Travis, and A. A. Lacis, *Scattering, Absorption, and Emission of Light by Small Particles* (Cambridge University Press, Cambridge, 2002).
[31] W. C. Chew, *Waves and Fields in Inhomogenous Media* (IEEE, Piscataway, NJ, 1995).
[32] W. Suh, Z. Wang, and S. Fan, IEEE J. Quantum Electron. **40**, 1511 (2004).